All-optical Switch Consisting of Multimode Interferometer Combined with Metamaterials: Device Design

Tomohiro Amemiya [1], Takahiko Shindo [2], Daisuke Takahashi [2], Nobuhiko Nishiyama [2], and Shigehisa Arai [1, 2]
1: Quantum Nanoelectronics Research Center, Tokyo Institute of Technology
2: Department Electrical and Electronic Enginnering, Tokyo Institute of Technology
2-12-1 O-okayama, Meguro-ku, Tokyo 152-8552, Japan
E-mail: amemiya.t.ab@m.titech.ac.jp, arai@pe.titech.ac.jp

Abstract

We demonstrated magnetically excited magnetic resonances with negative magnetic permeability in InP-based optical waveguide with an array of gold split-ring resonators (SRRs). In transmission characteristics of the device, an incident-polarization-dependent absorption feature was clearly observed at 1575 nm. The experimental results show that the SRR array interacted with the magnetic field of the propagating light in the device, producing magnetic resonance at optical frequencies.

Keywords- Integrated optics, Meta-materials, Waveguide device, III-V semiconductor

I. Introduction

The relative permeability of every natural material is 1 at optical frequency. However, if we can break this restriction, we will be able to find a new field in optical-communication device technology. This can be achieved using the concept of left-handed materials (LHMs), or metamaterials, which have attracted growing attention in recent years [1-5]. To examine the feasibility of such LHM optical devices, we designed and made a 1.5-μm-band, all-optical switch consisting of a semiconductor waveguide with a LHM region and confirmed magnetic interaction between the LHM and light that traveled in the waveguide. The following provides the outline of the device and the experimental results.

II. Theory and Design of LHM

Figure 1 shows the proposed optical switch composed of an GaInAsP/InP 1×1 multimode-interferometer (MMI) coupler and a LHM region consisting of gold split-ring-resonator (SRR) array attached on the coupler. For input TE-mode light with a frequency equal to SRR resonance frequency, the imaginary part of the permeability of the LHM region has a large absolute value, and this causes a large propagation loss of the input light. Then, if controlling light ($\lambda < \lambda_{g\_InP}$) is applied to the LHM region from above the device, a gap of each SRR is short-circuited by excited carriers in InP cladding layer, and consequently the magnetic response of the LHM region vanishes. This makes the imaginary part of the LHM permeability 0, thereby decreasing the propagation loss of the input light. In this way, the input light can be switched directly by the controlling light. (Our device can also have a function of light trapping due to a negative Goos-Hanchen shift caused by LHMs, therefore can be used as an optical memory.)

The magnetic properties of the LHM greatly depend on the conduction characteristics of metal that forms the SRRs.

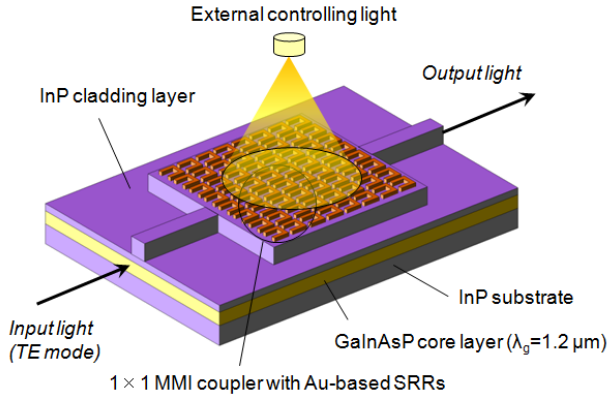

Fig 1 All-optical waveguide switch consisting of InP-based 1×1 MMI coupler covered with LHM (array of gold SRRs).

Therefore, we first calculated the dispersion of internal impedance (the ratio of surface electric field to total current) in gold (see [6, 7] for the formula for internal impedance at optical frequencies). Figure 2 shows the result for a gold layer with a thickness larger than the penetration depth at each frequency. As frequency increases, the real part of the internal impedance first increases steeply and then saturates at the inherent frequency, about 10 THz. At frequencies more than 100 THz, the real part gradually decreases, and this dispersion propertiy corresponds to the dielectric behavior of gold. In contrast, the imaginary part shows no saturation and has a large negative value at optical frequencies. This corresponds to ohmic loss in gold.

Using these results, we designed a SRR that had optical resonant frequency. For our device, a 4-cut single SRR (s-SRR) consisting of a gold square ring with four gaps (see left inset in Fig. 3) was used because this structure has a high resonant frequency due to its small gap capacitance [7]. From the Maxwell's equations and Biot-Savart law, we obtained equation

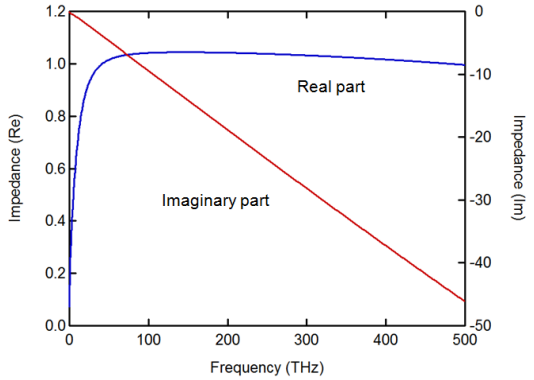

Fig 2 Internal impedance of gold as a function of frequency.

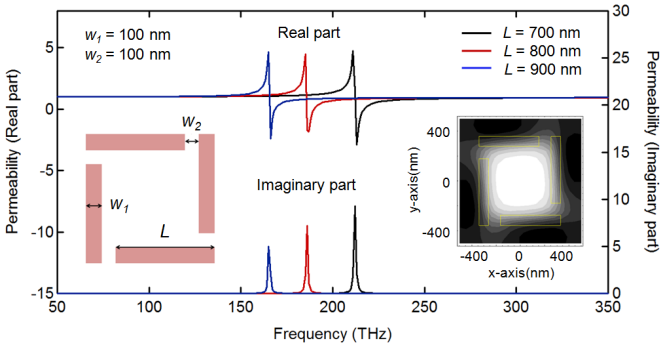

Fig 3 Complex permeability of LHM consisting of SRR array (d = 1.6 μm): (left inset) 4-cut single SRR, (right inset) magnetic field in gold SRR (L = 800 nm) at 185 THz.

$$\partial_t \int_{SRR} B d\sigma = i\omega\mu_0 \int_{SRR} \left(H_{ext} + \frac{1}{4\pi} \oint \frac{j d\mathbf{s} \times \mathbf{r}}{r^3} \right) d\sigma$$
$$= V_{ring} + 4V_{gap} = \left[Z(\tau) \cdot \frac{L}{W_1} - \frac{4W_2}{i\omega\varepsilon_0\varepsilon_m W_1 \tau} \right] j \quad , \qquad (1)$$

where H_{ext} is the magnetic field of light that travel in the device, ε_m and $Z(\tau)$ are the relative permittivity and internal impedance of gold, τ is a thickness of the SRR, j is induced current in the SRR, and L, W_1 and W_2 are the dimensions of the SRR (see left inset in Fig. 3).

Using Eq. (1), the distribution of magnetic field around the SRR was calculated, as illustrated with right inset in Fig. 3. From this result, we finally obtained the complex permeability $\bar{\mu}_{zz}$ of a LHM consisting of a SRR array, using the field averaging equation [8] given by

$$\bar{\mu}_{zz} = \frac{\bar{B}_z(0,0,d)}{\bar{H}_z(0,0,d)} = \mu_0 \frac{(2d)^{-2} \int_{-d}^{d} dx \int_{-d}^{d} H_z(x,y,d) dy}{(2d)^{-1} \int_0^{2d} H_z(0,0,z) dz} \quad , \qquad (2)$$

where d is the distance between SRRs, and B_z and H_z with over-lines represent the average values of magnetic flux density and magnetic field in the unit cell that includes a SRR. Figure 3(c) shows the results, with SRR size L as a parameter. Other parameters W_1 and W_2 were set to 100 nm, distance d between SRRs was set to 1.6 μm, and thickness τ was set twice as large

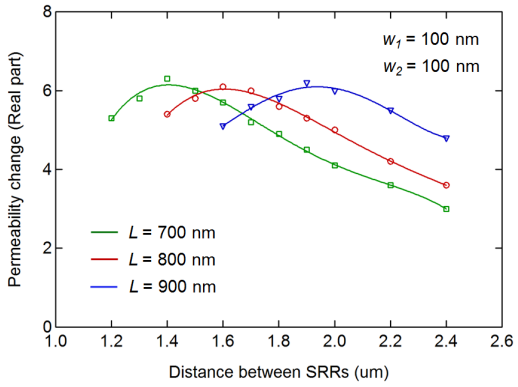

Fig 4 Permeability change as a function of distance between SRRs., calculated for 185 THz resonance.

as the penetration depth of gold at each frequency. The figure shows that SRRs with L = 700-800 nm show magnetic response at 1.5-μm-band frequencies.

The magnetic response of the LHM depends on distance d between SRRs. Figure 4 shows the intensity of magnetic response (i.e., change in permeability) as a function of d. In simulation, we considered nearest and next-nearest neighbor interaction between SRRs. There is an optimal distance that maximizes the magnetic response. For large distances, the response is weak because the surface density of SRRs is small. For small distances, magnetic field in a SRR is canceled by those of neighboring SRRs, and this weakens the total response of the SRR array.

III. Simulating Device Operation

After calculating the complex permeability of SRR-array layer, we designed a sample device and confirmed its operation with the aid of computer simulation based on the transfer-matrix method. We assumed that the device was composed of an undoped GaInAsP core layer (λ_g = 1.2 μm, n = 3.38, 200-nm thick) and an undoped InP cladding layer (n=3.16, 500-nm thick) formed on an InP substrate. A SRR array (L = 750 nm, W_1 = 100 nm, W_2 = 100 nm, d = 1.6 μm) with 1.5-μm-resonant frequency was attached on the surface of the cladding layer of the MMI region. The width and length of the MMI were set to 15 μm and 650 μm, respectively.

From Maxwell's equations, we obtained the transfer matrix with terms for permeability. Magnetic field $H_z^i(y)$ and electric field $E_x^i(y)$ in i-th layer can be given by equation

$$\begin{pmatrix} E_x^i(y) \\ H_z^i(y) \end{pmatrix} = \begin{pmatrix} \cosh[\beta_i(y-y_i)] & \frac{\mu_0\mu_i\omega}{j\beta_i}\sinh[\beta_i(y-y_i)] \\ -j\beta_i \sinh[\beta_i(y-y_i)] & \mu_0\mu_i\omega\cosh[\beta_i(y-y_i)] \end{pmatrix} \begin{pmatrix} E_x^i(y_i) \\ H_z^i(y_i) \end{pmatrix} \quad (3)$$

where y_i and μ_i are the bottom coordinate and complex permeability in i-th layer. Using Eq. (3) and boundary conditions for E_x and H_z, we can obtain the eigenvalue equation and calculate the propagation coefficient in each region of the MMI. In calculation, E_x and H_z were assumed to show exponential attenuation in the outside of the GaInAsP core layer (i.e., in air and the InP substrate).

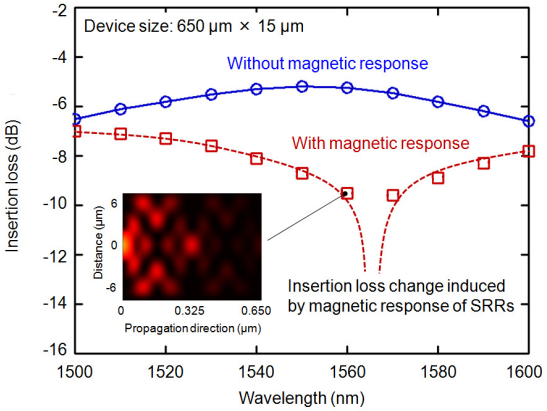

Fig. 5 Extinction ratio in sample device (L = 750 nm, W_1 = 100 nm, W_2 = 100 nm, d = 1.6 μm) as a function of wavelength. Inset shows electric field distribution in 1×1 MMI with SRR array.

Using the propagation coefficients, we calculated the propagation loss of light in the device as a function of wavelength. Figure 5 shows the results with SRR magnetic response (with SRR gaps open) and without the response (with SRR gaps shorted). A switching change in propagation loss of 4.2 dB or larger can be expected at 1560-1570 nm wavelength (corresponding to the SRR resonance frequency). In this way, waveguide-based switching device with LHMs can be realized for optical frequency.

IV. Device Fabrication and Characteristics

To move one step closer to actual all-optical switches, we made a trial device to confirm the magnetic response of the LHM consisting of s-SRRs arrayed on a GaInAsP/InP MMI coupler. The trial device was fabricated as follows. A starting material was a semi-insulating InP(100) wafer. An undoped GaInAsP core layer (λ_g = 1.2 μm, 200-nm thick) and an undoped InP cladding layer (500-nm thick) were grown in this order with organic-metal vapor phase epitaxy (OMVPE). On the surface of the cladding layer, s-SRRs consisting of Ti (5 nm) and Au (20 nm) layers were made using electron-beam (EB) lithography and lift-off process. Figures 6 show enlarged oblique views of the fabricated SRR array. The dimensions of the SRR were set to the values we used for the simulation in the previous sections.

After that, to make the 1×1 MMI coupler, a SiO_2 mask (100-nm thick) was formed on the wafer, using plasma-enhanced chemical vapor deposition (PECVD) and EB lithography. Then, the MMI coupler was formed using reactive ion etching with CH_4/H_2 mixture. Figure 7 shows the optical microscope view of the entire device, and enlarged cross-section views observed with SEM.

To examine the interaction of the SRRs and light traveling in the MMI, we measured the transmission characteristics of the device. The light from a tunable laser was transferred into and out of the device through a polarization controller (see Fig. 8(a)). We first measured near field patterns at the output end of the device and confirmed that the single-mode connection was

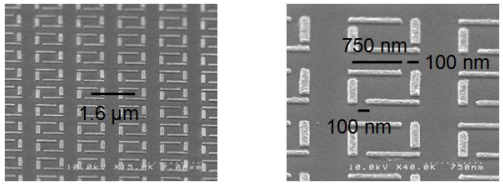

(a) (b)

Fig 6 SEM images of gold SRR array before SiO_2 deposition; (a) wide area view, and (b) enlarged view.

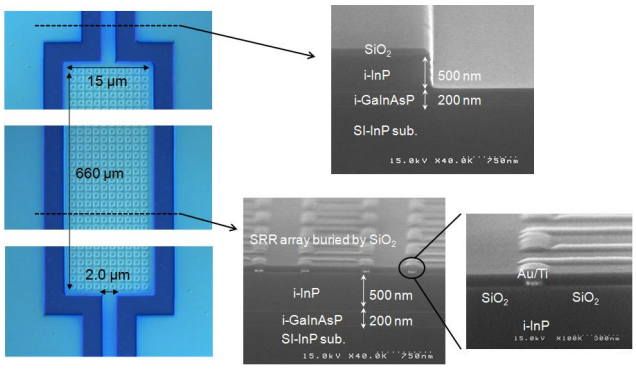

(a) (b)

Fig. 7 MMI coupler with gold SRRs covered with SiO_2 layer; (a) optical microscope image, and (b) SEM cross-section images.

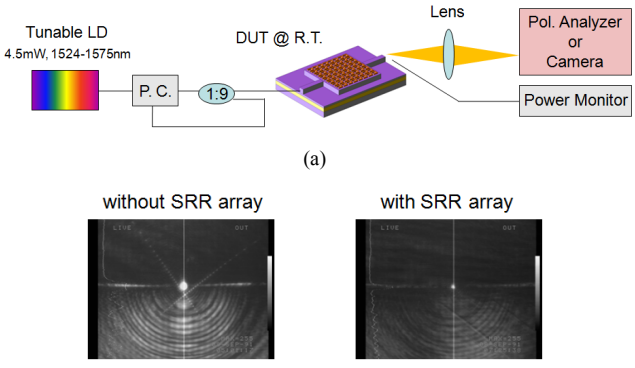

(a)

(b)

Fig. 8 (a) Measurement setup for 1×1 MMI coupler with gold SRR array. (b) Near field pattern of device with/without SRR array.

established (see Fig. 8(b)). Then, we measured the intensity of the output light, using a power meter. In this measurement, control devices without SRRs were also prepared for comparison. Figure 9 plots transmission intensity for devices with SRRs (blue curves) and without SRRs (black curves) as a function of wavelength from 1524 to 1575 nm, measured for input light of (a) TE mode and (b) TM mode. To clarify the effect of magnetic interaction between light and the SRRs, we took the difference between the transmission intensity with SRRs and that without SRRs (see red curves in the Fig. 5). As shown in Fig. 9, the magnetic interaction was observed only for TE-mode light; that is, the transmission intensity with SRRs gradually decreased with wavelength for TE mode. No decrease

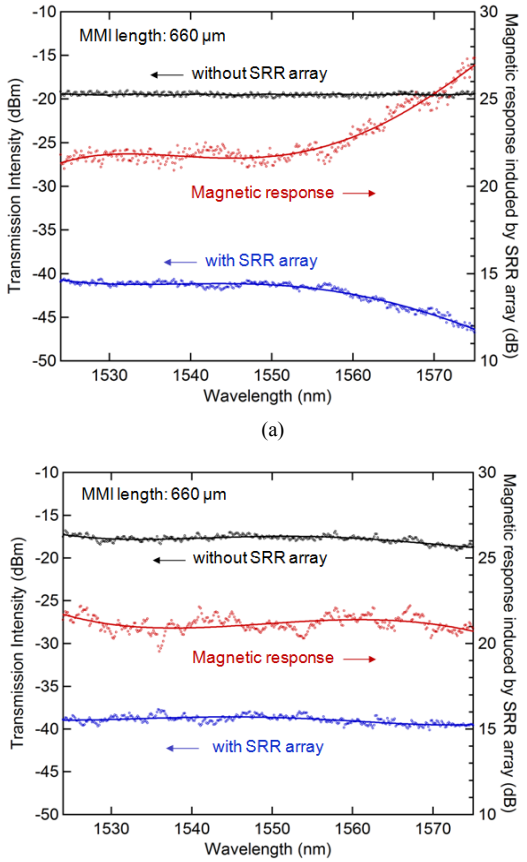

Fig. 9 Transmission intensity of devices with SRR (blue lines) and without SRRs (black lines) as a function of wavelength, measured for (a) TE mode and (b) TM mode. Difference between two devices is also plotted for both modes (red lines).

in intensity was observed for TM mode. This polarization-dependent absorption is positive proof that the magnetic field of light interacted with the SRRs to produce magnetic resonance at optical frequencies. (The frequency of resonance peak in this device shifted towards a longer wavelength than we had expected and was out of the measurement range because the host material for the SRRs in the experiment was SiO_2 and different from material (i.e., air) assumed in simulation.)

In Figs. 9(a) and 9(b), the difference between the transmission intensity at 1524 nm and that at 1575 nm is an index of the magnetic response of the LHM. We measured this difference as a function of MMI length. The result is plotted in Fig. 10, showing that the magnetic response can be observed only for TE-mode light.

V. Conclusion

We fabricated an InP-based optical waveguide device combined with left-handed material (metamaterial) and demonstrated magnetic interaction with the metamaterial and light that traveled in the waveguide. The metamaterial consists of an array of

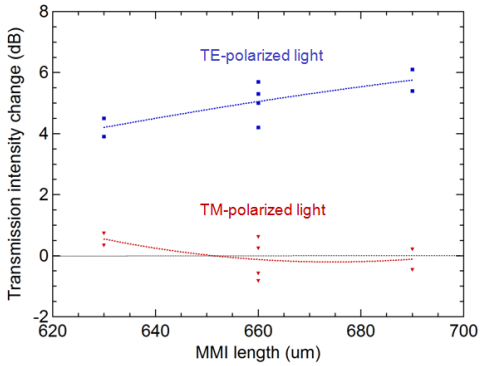

Fig. 10 Difference between 1524-nm transmission intensity and 1575-nm one as a function of MMI length, measured for TE and TM mode.

minute metal split-ring resonators (SRRs) attached on the waveguide. The operation wavelength is set to 1.5 μm. The transmission characteristics of the device strongly depend on the polarization and wavelength of input light. This shows that the SRR array interacted with the magnetic field of light and produced magnetic resonance at optical frequencies. Our result is useful to develop waveguide-based matamaterial devices for optical communication.

Acknowledgment

This research was financially supported by a Grant-in-Aid for Scientific Research (#19002009, #19686023, and #21860031) from the Ministry of Education, Culture, Sports, Science and Technology, Japan (MEXT).

References

[1] R. M. Walser, "Electromagnetic Metamaterials," *Proc. SPIE*, Vol. 4467, pp. 1-15, July 2001.

[2] H. T. Chen, W. J. Padilla , Joshua M. O. Zide, A. C. Gossard, A. J. Taylor, and R. D. Averitt, "Active Terahertz Metamaterial devices," *Nature*, Vol. 444, No. 7119, pp. 597-600, Nov. 2006.

[3] S. Linden, C. Enkrich, G. Dolling, M. Klein, J. Zhou, T. Koschny, C. Soukoulis, S. Burger, F. Schmidt, and M. Wegener, "Photonic Metamaterials: Magnetism at Optical Frequencies (invited paper)," *IEEE J. Sel. Top. Quantum Electron.,* Vol. 12, No. 4, pp. 1097-1105, Nov./Dec. 2006.

[4] W. Cai, U. K. Chettiar, Hsiao-Kuan Yuan, V. C. de Silva, A. V. Kildishev, V. P. Drachev, and V. M. Shalaev, "Metamagnetics with Rainbow Colors," *Opt. Express*, Vol. 15, No. 6, pp. 3333-3341, Mar. 2007.

[5] H. J. Lezec, J. A. Dionne, and H. A. Atwater, "Negative Refraction at Visible Frequencies," *Science*, Vol. 316, No. 5823, pp. 430-432, Apr. 2007.

[6] S. Ramo, J. R. Whinnery, and T. Van Duzer, *Field and Waves in Communication Electronics (Wiley 1993)*, pp. 149-153.

[7] A. Ishikawa, T. Tanaka, and S. Kawata, "Frequency Dependence of the Magnetic Response of Split-ring Resonators, " *J. Opt. Soc. Am. B*, Vol. 24, No. 3, pp. 510-515, Mar. 2007.

[8] D. R. Smith and J. B. Pendry, "Homogenization of Metamaterials by Field Averaging (invited paper), " *J. Opt. Soc. Am B*, Vol. 23, No. 3, pp. 391-403, Mar. 2006.